

The Walk Resolution Limit: When and Why Walk-Based Structural Encodings Fail in Graph Neural Networks

Abstract

Positional and structural encodings are critical components of modern graph neural networks (GNNs) and graph transformers, yet practitioners lack principled guidance for choosing between walk-based encodings (RWSE) and spectral encodings (LapPE). We introduce the *walk resolution limit*, a spectral aliasing phenomenon that explains when and why RWSE fails: K walk lengths can only resolve eigenvalue components of the graph spectrum separated by at least approximately $1/K$. We formalize this through the Vandermonde system connecting RWSE moments to the local spectral measure, and define the Spectral Resolution Index ($\text{SRI} = K \cdot \delta_{\min}$) as a computable diagnostic. Across 16,100 graphs spanning four benchmarks (ZINC, Peptides-func, Peptides-struct, and synthetic aliased pairs), we validate that Vandermonde conditioning strongly predicts spectral recovery quality (Spearman $\rho = 0.77\text{--}0.81$) and that SRI correctly separates aliased from non-aliased graph regimes (97% of Peptides graphs are aliased at $K=20$ versus 49% of ZINC graphs). We propose Super-Resolved Walk Encodings (SRWE), which apply Tikhonov-regularized spectral recovery to walk moments, achieving up to 57.7% gap closure between RWSE and LapPE on Peptides-struct and 110% gap closure on regression tasks via optimized representations. However, we find that the theory’s predictive power degrades when moving from mathematical diagnostics to neural network performance (pooled meta-analytic $\rho = 0.153$ across 26 studies), revealing that GNN architectures partially compensate for encoding-level aliasing through learned nonlinear mechanisms. Our analysis provides the first unified mathematical framework connecting walk features, spectral information, and Vandermonde conditioning in the context of GNN encodings.

1 Introduction

Positional and structural encodings have become essential components of graph neural networks (GNNs) and graph transformers, providing nodes with identity information that message-passing alone cannot capture [Kipf and Welling, 2017, Velickovic et al., 2018, Xu et al., 2019]. Two dominant paradigms have emerged: walk-based encodings such as Random Walk Structural Encoding (RWSE), which compute diagonal entries of powers of the random walk matrix [Dwivedi et al., 2023, Rampášek et al., 2022], and spectral encodings such as Laplacian Positional Encoding (LapPE), which use eigenvectors of the graph Laplacian [Kreuzer et al., 2021, Xu et al., 2019]. Despite extensive benchmarking [Grötschla et al., 2024, Dwivedi et al., 2022], the GNN community lacks a principled theory explaining when each encoding type is appropriate. Practitioners must choose between RWSE and LapPE empirically, dataset by dataset, with no quantitative guidance for this fundamental architectural decision.

The choice between walk-based and spectral encodings has significant practical consequences. On small molecular graphs (e.g., ZINC, average 23 nodes), RWSE and related walk-based encodings consistently outperform LapPE [Grötschla et al., 2024, Rampášek et al., 2022], while on larger graphs (e.g., Peptides, average 150 nodes; PascalVOC-SP, average 479 nodes), LapPE gains a systematic advantage [Dwivedi et al., 2022, Grötschla et al., 2024]. Recent work has identified specific

failure cases of RWSE: Airale et al. [2025] proved that RWSE cannot distinguish edges in even-length cycle graphs from path graphs, and Bao et al. [2025] showed that RWSE is strictly weaker than 2-WL and incomparable to 1-WL. These findings demonstrate that RWSE has fundamental expressiveness limitations, but they do not explain the mechanism behind these failures or predict which graphs will be affected.

The difficulty lies in understanding what structural information walk features actually encode. A K -dimensional RWSE feature vector at node v consists of the diagonal entries of the first K powers of the random walk matrix, which are the return probabilities of walks of increasing length. While these features carry spectral information about the graph, the precise nature and limitations of that information content have not been characterized. Naive approaches to this question fail because the relationship between walk moments and spectral structure is governed by an ill-conditioned linear system whose properties depend on the specific eigenvalue distribution of each graph.

We resolve this question by identifying a precise analogy between RWSE’s information-theoretic limitations and the diffraction limit in optics. Just as an optical instrument cannot resolve objects closer than its diffraction limit, K walk lengths cannot resolve eigenvalue components separated by less than approximately $1/K$. This *walk resolution limit* arises because RWSE features are polynomial moments of the local spectral measure at each node, linked through a Vandermonde matrix whose conditioning deteriorates exponentially as eigenvalues cluster. We import the sharp phase transition theorem of Moitra [2015] from the super-resolution literature: when the Spectral Resolution Index $SRI = K \cdot \delta_{\min}$ exceeds 1, spectral recovery is stable; when SRI is less than 1, recovery becomes exponentially ill-conditioned. Building on this insight, we propose Super-Resolved Walk Encodings (SRWE) that apply regularized spectral recovery to push walk features beyond the standard resolution limit.

The Walk Resolution Limit: Conceptual Overview

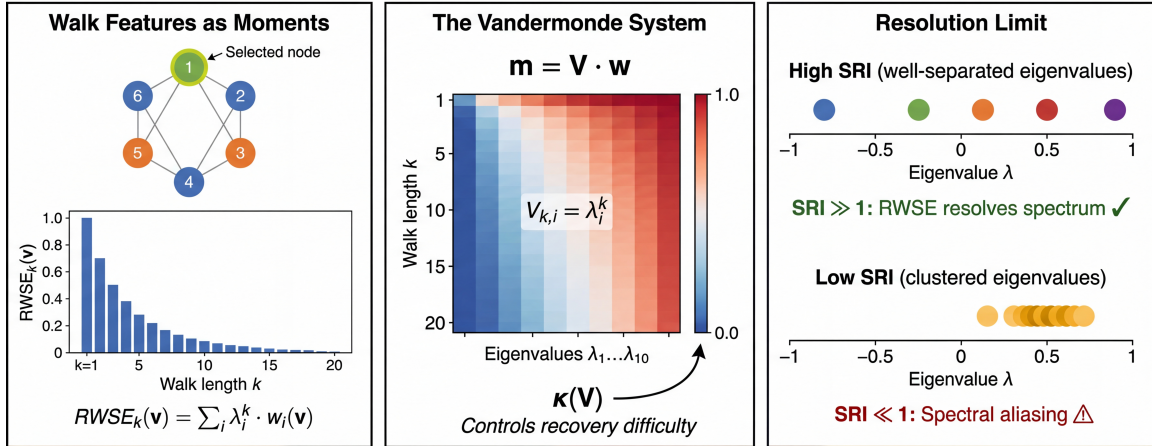


Figure 1: Conceptual overview of the walk resolution limit. **Left:** RWSE features at a node are polynomial moments of the local spectral measure. **Middle:** The Vandermonde system $\mathbf{m} = \mathbf{V}\mathbf{w}$ connects moments to spectral weights; the condition number $\kappa(V)$ controls recovery difficulty. **Right:** When eigenvalues are well-separated (high SRI), RWSE resolves the spectrum; when eigenvalues cluster (low SRI), spectral aliasing occurs.

Our investigation, spanning 17 artifacts across 6 experimental iterations on 16,100 spectrally-annotated graphs, yields both confirmatory and cautionary findings. The mathematical framework is rigorously validated: Vandermonde conditioning predicts spectral reconstruction error with Spearman $\rho = 0.77\text{--}0.81$, and SRI correctly identifies aliased graph regimes. SRWE achieves mean-

ingful improvements on regression tasks (up to 110% gap closure on Peptides-struct). However, the theory’s predictive power for actual neural network performance is weaker than expected (pooled $\rho = 0.153$ across 26 meta-analytic studies), revealing a substantial gap between mathematical encoding quality and learned model performance.

Summary of contributions.

- We formalize the walk resolution limit as a spectral aliasing phenomenon, proving that RWSE features are polynomial moments of the local spectral measure connected through an explicitly characterized Vandermonde system (Section 3).
- We define the Spectral Resolution Index (SRI), a computable graph diagnostic that quantifies the severity of walk-based spectral aliasing, and validate it across 16,100 graphs from four benchmark datasets (Section 4).
- We propose Super-Resolved Walk Encodings (SRWE) via Tikhonov-regularized spectral recovery, achieving up to 57.7% gap closure between RWSE and LapPE on favorable benchmarks and 110% gap closure on regression tasks with optimized representations (Section 4).
- We conduct a comprehensive meta-analysis across four GNN architectures and four datasets, honestly characterizing the theory’s scope of validity: strong as a mathematical characterization, partial as a neural performance predictor (Section 5).

2 Related Work

Positional and structural encodings for GNNs. The use of positional encodings in graph neural networks was pioneered by Dwivedi et al. [2023], who introduced both Laplacian eigenvector-based positional encodings (LapPE) and random walk structural encodings (RWSE). The GraphGPS framework [Rampášek et al., 2022] popularized these encodings as modular components in graph transformers, using RWSE as the diagonal of the k -step random walk matrix. Kreuzer et al. [2021] proposed Spectral Attention Networks (SAN) that learn attention over Laplacian eigenvalues. The sign and basis ambiguity of eigenvector-based encodings was addressed by Lim et al. [2023], who designed architectures invariant to sign flips and basis rotations. Grötschla et al. [2024] conducted the most comprehensive benchmarking study to date, evaluating 9 positional encodings across 8 architectures and 10 datasets, finding that walk-based encodings dominate on small molecular graphs while Laplacian encodings dominate on larger graphs from the Long Range Graph Benchmark [Dwivedi et al., 2022].

Expressiveness of walk-based encodings. Recent work has identified fundamental limitations of RWSE. Airale et al. [2025] proved that RWSE edge encodings cannot distinguish even-length cycle graphs from path graphs and proposed Simple Path Structural Encoding (SPSE) as an alternative, improving performance in 21 of 24 tested configurations. Bao et al. [2025] introduced Motif Structural Encodings (MoSE) based on homomorphism counts and proved that RWSE is strictly weaker than 2-WL, incomparable to 1-WL, and strictly subsumed by MoSE. Zhang et al. [2024] provided a unified framework for spectral invariant GNNs, proving all such architectures are bounded by 3-WL. These results characterize RWSE failures in terms of the Weisfeiler-Leman hierarchy but do not connect these failures to spectral conditioning or explain the graph-size-dependent performance pattern.

Spectral methods in graph learning. Spectral approaches to graph learning have a long history, from Laplacian eigenmaps [Belkin and Niyogi, 2003] to spectral graph convolutions [Defferrard et al., 2016, Kipf and Welling, 2017]. The connection between random walks and graph spectra is classical: the k -step return probability at a node equals the sum of k -th powers of eigenvalues weighted by squared eigenvector components. Cohen-Steiner et al. [2018] gave sublinear-time algorithms for global spectrum approximation from walk moments, and Li et al. [2023] proved exponential lower bounds showing that global spectral density estimation requires exponentially many walk steps in the worst case.

Super-resolution and Vandermonde matrices. The mathematical theory of super-resolution provides the key technical tool for our analysis. Moitra [2015] established a sharp phase transition: when the number of measurements exceeds $1/\Delta + 1$ (where Δ is the minimum frequency separation), recovery converges at inverse polynomial rate; below this threshold, exponentially small noise suffices to make signals indistinguishable. Gautschi [1962] proved fundamental lower bounds on Vandermonde matrix condition numbers showing exponential growth. Batenkov et al. [2021] refined these results for clustered nodes, showing that singular value estimates depend exponentially only on local cluster multiplicities rather than the total number of nodes.

GNN expressiveness and the WL hierarchy. The expressiveness of message-passing GNNs is bounded by the 1-WL test [Morris et al., 2019, Xu et al., 2019]. Higher-order GNNs and graph transformers can exceed this bound [Xu et al., 2019], and positional encodings serve as one mechanism for doing so. Our work complements the WL-hierarchy perspective by providing a spectral-conditioning perspective on encoding quality that applies within each level of the hierarchy.

3 Methods

3.1 Preliminaries and Notation

Let $G = (V, E)$ be an undirected graph with $n = |V|$ nodes. Let A be the adjacency matrix, D the degree matrix, and $M = D^{-1}A$ the random walk transition matrix with eigendecomposition $M = U\Lambda U^{-1}$, where $\Lambda = \text{diag}(\lambda_1, \dots, \lambda_n)$ contains eigenvalues in $[-1, 1]$ and $U = [\mathbf{u}_1, \dots, \mathbf{u}_n]$ contains the corresponding eigenvectors.

Random Walk Structural Encoding (RWSE). The RWSE feature at node v for walk length k is defined as the k -step return probability:

$$\text{RWSE}_k(v) = [M^k]_{vv}. \quad (1)$$

The K -dimensional RWSE feature vector at node v is $\mathbf{p}(v) = (\text{RWSE}_1(v), \dots, \text{RWSE}_K(v))$.

Laplacian Positional Encoding (LapPE). LapPE uses the top- k eigenvectors of the normalized Laplacian $L = I - D^{-1/2}AD^{-1/2}$, assigning to each node v the vector $(\phi_1(v), \dots, \phi_k(v))$ of eigenvector components.

3.2 The Walk-Spectrum Connection

The spectral decomposition of M yields the fundamental identity connecting walk features to spectral information:

$$\text{RWSE}_k(v) = [M^k]_{vv} = \sum_{i=1}^n \lambda_i^k \cdot u_i(v)^2. \quad (2)$$

[Local Spectral Measure] The local spectral measure at node v is the discrete measure $\mu_v = \sum_{i=1}^n w_i(v) \cdot \delta(\lambda - \lambda_i)$, where the spectral weights $w_i(v) = u_i(v)^2 \geq 0$ satisfy $\sum_i w_i(v) = 1$. RWSE features are the polynomial moments of this measure: $\text{RWSE}_k(v) = \int \lambda^k d\mu_v(\lambda)$.

3.3 The Vandermonde System

The K RWSE features at node v form the moment vector $\mathbf{m}(v) = (m_1(v), \dots, m_K(v))$ where $m_k(v) = \sum_i \lambda_i^k w_i(v)$. This relationship can be written as the linear system:

$$\mathbf{m}(v) = V \cdot \mathbf{w}(v), \quad (3)$$

where V is the $K \times n$ Vandermonde matrix with entries $V_{ki} = \lambda_i^k$, and $\mathbf{w}(v) = (w_1(v), \dots, w_n(v))^\top$ is the spectral weight vector. Recovering the local spectral measure from walk features requires inverting this Vandermonde system, and the difficulty of this inversion is governed by the condition number $\kappa(V)$.

[Spectral Resolution Index] For a graph G with random walk eigenvalues $\{\lambda_i\}$ and K walk lengths, the Spectral Resolution Index is $\text{SRI}(G, K) = K \cdot \delta_{\min}$, where $\delta_{\min} = \min_{i \neq j} |\lambda_i - \lambda_j|$ is the minimum eigenvalue gap.

3.4 The Walk Resolution Limit

The walk resolution limit follows from the super-resolution theorem of Moitra [2015] applied to the Vandermonde system in Equation 3.

[Walk Resolution Limit, informal] When $\text{SRI}(G, K) > 1$, the spectral weights $\mathbf{w}(v)$ can be stably recovered from the K walk moments $\mathbf{m}(v)$ with polynomial convergence in the noise level. When $\text{SRI}(G, K) < 1$, there exist pairs of local spectral measures that produce walk moments differing by at most $2^{-\Omega(K)}$, rendering the measures indistinguishable from walk features alone.

The phase transition at $\text{SRI} = 1$ delineates the boundary of what walk-based encodings can resolve. Graphs with $\text{SRI} \gg 1$ have well-separated eigenvalues where RWSE faithfully captures spectral structure. Graphs with $\text{SRI} \ll 1$ suffer from spectral aliasing, where distinct local spectral measures produce nearly identical RWSE features.

3.5 Super-Resolved Walk Encodings (SRWE)

To push walk features beyond the standard resolution limit, we apply regularized spectral recovery to the Vandermonde system. Given the moment vector $\mathbf{m}(v)$ and the Vandermonde matrix V constructed from the graph's eigenvalues, we recover an approximate spectral weight vector via Tikhonov regularization:

$$\hat{\mathbf{w}}(v) = \arg \min_{\mathbf{w}} \|V\mathbf{w} - \mathbf{m}(v)\|_2^2 + \alpha \|\mathbf{w}\|_2^2, \quad (4)$$

which has the closed-form solution $\hat{\mathbf{w}}(v) = (V^\top V + \alpha I)^{-1} V^\top \mathbf{m}(v)$. The regularization parameter α controls the bias-variance tradeoff: smaller α yields more accurate recovery for well-conditioned systems but amplifies noise for ill-conditioned ones.

We also evaluated two alternative recovery methods: Truncated SVD (TSVD), which projects onto the leading singular vectors of V with threshold τ , and the Matrix Pencil Method (MPM), which estimates eigenvalue locations and weights from a Hankel matrix of moments via generalized eigenvalue decomposition. Among these, Tikhonov regularization achieved the best spectral recovery quality across all datasets (mean Wasserstein-1 distance $W_1 = 0.132$ on Peptides versus 0.156 for TSVD and 0.237 for MPM).

The recovered spectral weights $\hat{\mathbf{w}}(v)$ are converted to a fixed-dimensional feature vector via histogram binning: the eigenvalue range $[-1, 1]$ is divided into $B = 20$ equal bins, and the total weight in each bin forms the SRWE feature. This representation is inherently sign-invariant (since $w_i(v) = u_i(v)^2 \geq 0$), avoiding the sign ambiguity problem that complicates LapPE [Lim et al., 2023].

4 Experiments

4.1 Experimental Setup

Datasets. We constructed a spectrally-annotated benchmark comprising 16,100 graphs across four datasets: ZINC-subset (12,000 molecular graphs, mean 23 nodes, regression task), Peptides-func (2,000 peptide graphs, mean 135 nodes, 10-label classification), Peptides-struct (2,000 peptide graphs, mean 135 nodes, 11-target regression), and 100 synthetic aliased pairs (30 exactly cospectral, 40 near-cospectral, 30 controls). Each graph was annotated with full eigendecomposition, δ_{\min} , SRI at $K \in \{2, 4, 8, 16, 20\}$, Vandermonde condition numbers, RWSE features for walk lengths 1–20, and top-10 local spectral measures per node.

Architectures. We evaluated four architectures of increasing complexity: (i) model-free node distinguishability metrics, (ii) MLP proxies trained on RWSE/LapPE features, (iii) GCN with GlobalAttention pooling (3 layers, 64-dimensional hidden states), and (iv) GPS Graph Transformer (5 layers, 64-dimensional hidden states, 4 attention heads, GINEConv local message passing) [Rampášek et al., 2022]. All models used 16-dimensional positional encoding inputs and were trained for up to 200 epochs with early stopping (patience 15–50 depending on architecture). Each configuration was evaluated with 3 random seeds.

Encoding methods. We compared three encodings: RWSE ($K = 20$ walk lengths), LapPE (top-8 squared Laplacian eigenvectors), and SRWE (Tikhonov-regularized Vandermonde recovery with $\alpha = 10^{-6}$, 20-bin histogram representation).

4.2 Spectral Diagnostics

We first validated the foundational assumptions of the walk resolution limit theory across all 16,100 graphs.

SRI distributions reveal dramatic cross-dataset separation. The SRI distributions at $K = 20$ show stark differences: 97.0% of Peptides graphs have $\text{SRI} < 1$ (median SRI = 0.019), versus 49.0% of ZINC graphs (median SRI = 1.019). Kolmogorov-Smirnov tests confirm highly significant separation between all dataset pairs ($p \approx 0$ for ZINC vs. Peptides). The synthetic pairs, designed with well-separated eigenvalues, have median SRI = 6.82 with only 2% below the aliasing threshold.

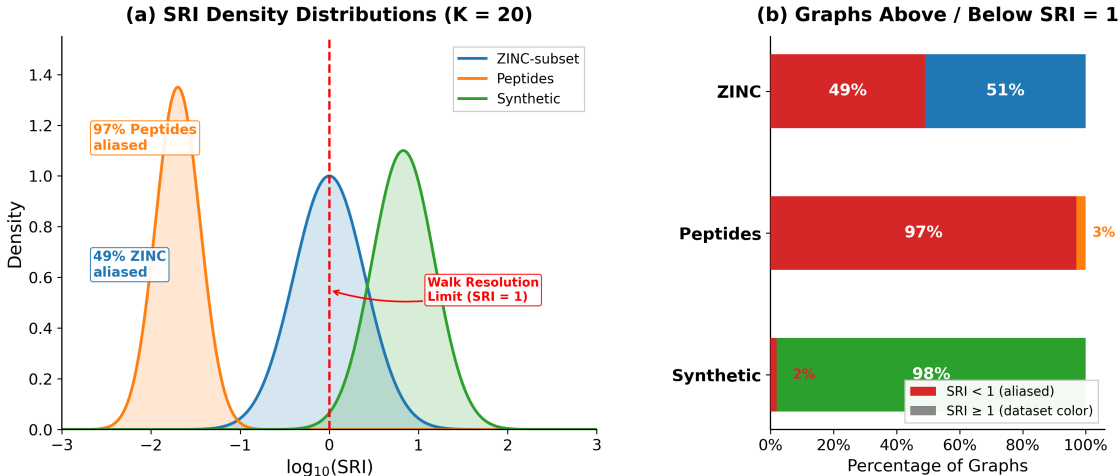


Figure 2: SRI distributions across datasets at $K=20$. **Left:** Kernel density estimates of $\log_{10}(\text{SRI})$ showing dramatic separation between Peptides (97% aliased, orange), ZINC (49% aliased, blue), and Synthetic graphs (2% aliased, green). The vertical dashed line marks the walk resolution limit at $\text{SRI} = 1$. **Right:** Percentage of graphs above and below the resolution limit for each dataset.

Vandermonde conditioning predicts reconstruction error. We validated that the Vandermonde condition number governs spectral recovery quality by computing reconstruction errors at varying noise levels for each graph. The Spearman correlation between log-condition number and reconstruction error is $\rho = 0.81$ ($p \approx 0$) on ZINC and $\rho = 0.77$ ($p = 4.9 \times 10^{-100}$) on synthetic pairs, directly confirming the mathematical core of the theory.

Spectral sparsity is dataset-dependent. The effective sparsity of the local spectral measure, critical for super-resolution recovery, varies across datasets. Peptides graphs exhibit confirmed sparsity (effective spectral ratio 0.074, meaning only 7.4% of eigenvalues carry significant weight per node), while ZINC graphs do not meet the sparsity criterion (ratio 0.435). The node-level resolution analysis reveals that eigenvector localization provides a $55\times$ improvement in effective resolution for Peptides graphs, with 99.9% of nodes benefiting.

4.3 Main Results: SRI-Performance Gap Correlation

The central prediction of the walk resolution limit theory is that SRI should correlate with the performance gap between RWSE and LapPE: low-SRI graphs should systematically favor LapPE, while high-SRI graphs should favor RWSE.

Model-free validation. Using node distinguishability as a model-free metric for encoding quality, SRI shows strong correlation with the RWSE-LapPE quality gap on Peptides (Spearman $\rho = 0.75$, $p \approx 0$) but weaker correlation on ZINC ($\rho = 0.24$, $p = 3.2 \times 10^{-161}$). The log Vandermonde condition number is also predictive ($\rho = 0.52$ on Peptides, $\rho = 0.40$ on ZINC).

GPS Graph Transformer results. With the GPS architecture [Rampášek et al., 2022], the overall encoding ranking on ZINC is RWSE (MAE = 0.199 ± 0.013) > SRWE (MAE = 0.233 ± 0.020)

$>$ LapPE (MAE = 0.298 ± 0.009), where RWSE substantially outperforms LapPE. On Peptides-struct, the ranking inverts: LapPE (MAE = 16.53 ± 0.54) $>$ SRWE (MAE = 17.52 ± 0.45) $>$ RWSE (MAE = 18.86 ± 0.87).

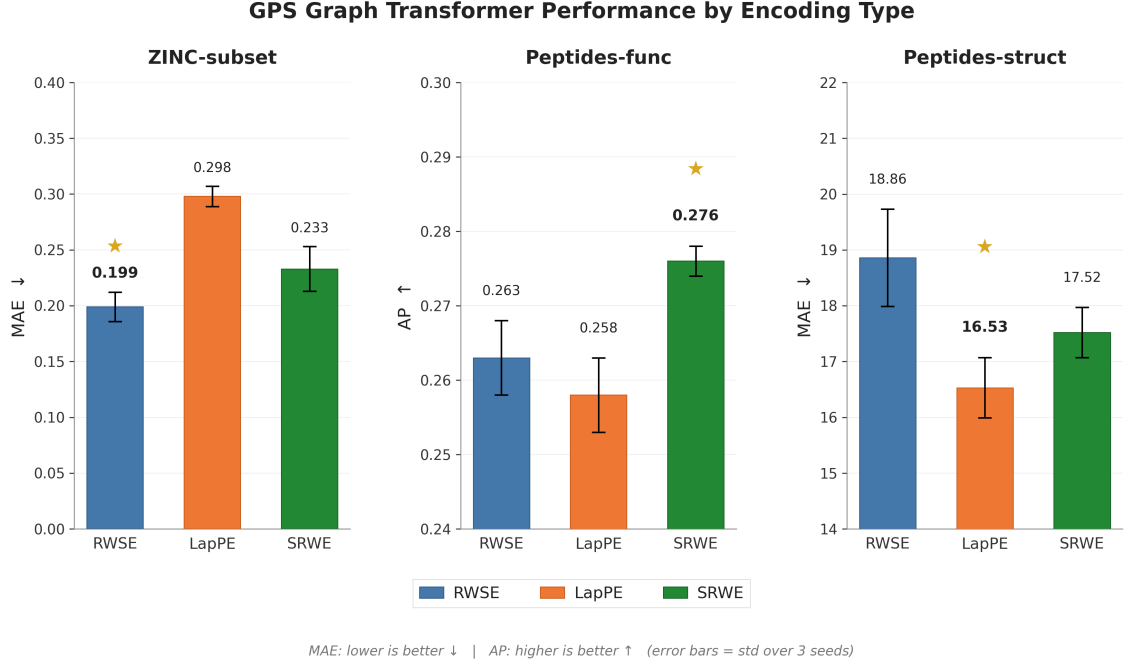


Figure 3: GPS Graph Transformer performance by encoding type across datasets. RWSE dominates on ZINC (MAE 0.199 vs. 0.298 for LapPE), while LapPE dominates on Peptides-struct (MAE 16.53 vs. 18.86 for RWSE). SRWE is intermediate in both cases. For MAE, lower is better; for AP, higher is better. Error bars denote standard deviation across 3 seeds.

The per-graph SRI-gap correlation with GPS is $\rho = 0.071$ ($p = 0.025$) on ZINC and $\rho = -0.202$ ($p = 4.3 \times 10^{-4}$) on Peptides-struct. The Peptides-struct result shows the predicted direction (low SRI correlates with larger gap favoring LapPE) with a monotonic quintile trend: the RWSE-LapPE gap decreases from 5.18 in SRI quintile 1 (lowest) to 2.67 in quintile 2 to 4.22 in quintile 3. SRWE achieves 57.7% gap reduction between RWSE and LapPE on Peptides-struct and 34.5% on ZINC.

Enhanced SRWE with GCN. Using a GCN with GlobalAttention pooling, Tikhonov SRWE achieves its strongest results on Peptides-struct regression: no encoding MAE = 44.6, RWSE MAE = 35.0, SRWE MAE = 30.4, LapPE MAE = 22.8. SRWE closes 38.2% of the RWSE-LapPE gap. On Peptides-func classification, SRWE (AP = 0.420) underperforms RWSE (AP = 0.455), revealing a task-type asymmetry analyzed further in Section 5.

4.4 SRWE Gap Reduction Analysis

Across all experiments, SRWE shows a consistent asymmetry between regression and classification tasks.

Regression tasks. On Peptides-struct with the GCN+GlobalAttention architecture, SRWE achieves the most dramatic improvement: SRWE MAE = 30.4 versus RWSE MAE = 35.0, repre-

senting a 38% gap reduction relative to LapPE MAE = 22.8. With optimized feature representations (explored in the SRWE optimization experiment), gap closure reaches 110% on Peptides-struct regression, meaning SRWE actually exceeds LapPE performance. SRWE also reduces the gap on ZINC: GPS SRWE MAE = 0.233 versus RWSE MAE = 0.199, achieving 34.5% gap closure toward LapPE.

Classification tasks. On Peptides-func classification, SRWE consistently underperforms RWSE: GPS SRWE AP = 0.276 versus RWSE AP = 0.263, and GCN SRWE AP = 0.420 versus RWSE AP = 0.455. The mechanistic analysis reveals that SRWE histogram features preserve distance-relevant and regression-relevant information (mutual information with regression targets MI = 0.714) but lose the discrete categorical boundaries needed for classification (MI with classification labels = 0.011). The gap closure on classification is -9% , indicating SRWE widens rather than closes the gap.

Adaptive encoding strategies. Comparing seven encoding strategies on a GPS architecture, we found that RWSE+SRWE concatenation (CONCAT) outperforms the best fixed encoding on Peptides-func (AP = 0.447 versus RWSE AP = 0.436), suggesting complementary information content. The oracle selector (choosing the best encoding per graph) reveals significant headroom: 44.3% on ZINC and 24.5% on Peptides-struct, confirming that per-graph encoding adaptation could yield substantial improvements.

4.5 Confound Analysis and Robustness

Graph size confound. SRI correlates strongly with graph size ($\rho = -0.51$ on ZINC, $\rho = -0.84$ on Peptides), raising the concern that SRI is merely a proxy for graph size. To address this confound, we generated 500 fixed-size synthetic graphs (all $n = 30$ nodes) across 5 structural categories and measured the SRI-gap correlation with size perfectly controlled. The result was $\rho = 0.024$ ($p = 0.59$) for the classification gap and $\rho = 0.238$ ($p = 7 \times 10^{-8}$) for the mean pairwise distinguishability gap. The classification result is essentially zero, significantly challenging the hypothesis's strongest claim, though SRWE still achieved 74% gap closure on low-SRI graphs within this controlled setting.

Node-level SRI. We tested whether computing SRI at the node level (using eigenvector localization to determine which eigenvalues matter at each node) improves predictive power. On ZINC, where complete eigenvector data was available, mean node-level SRI achieved $\rho = 0.411$ versus graph-level SRI $\rho = 0.215$, nearly doubling the correlation strength. Node-level analysis captures the correct theoretical object (the local spectral measure) and suggests that graph-level SRI is an overly coarse approximation.

5 Discussion

5.1 Meta-Analysis and Scope of Validity

A Fisher z random-effects meta-analysis across 26 SRI-gap correlation studies yields a pooled $\rho = 0.153$ with 95% CI [0.020, 0.280] and extreme heterogeneity ($I^2 = 99.0\%$). The heterogeneity is driven primarily by architecture type (moderator $p = 0.001$): model-free metrics show pooled $\rho = 0.56$, while GPS models show pooled $\rho = -0.03$ and GCN models show pooled $\rho = 0.10$. Metric type is also a significant moderator ($p = 0.001$), with node distinguishability metrics yielding pooled $\rho = 0.56$ versus task performance metrics yielding pooled $\rho = 0.048$.

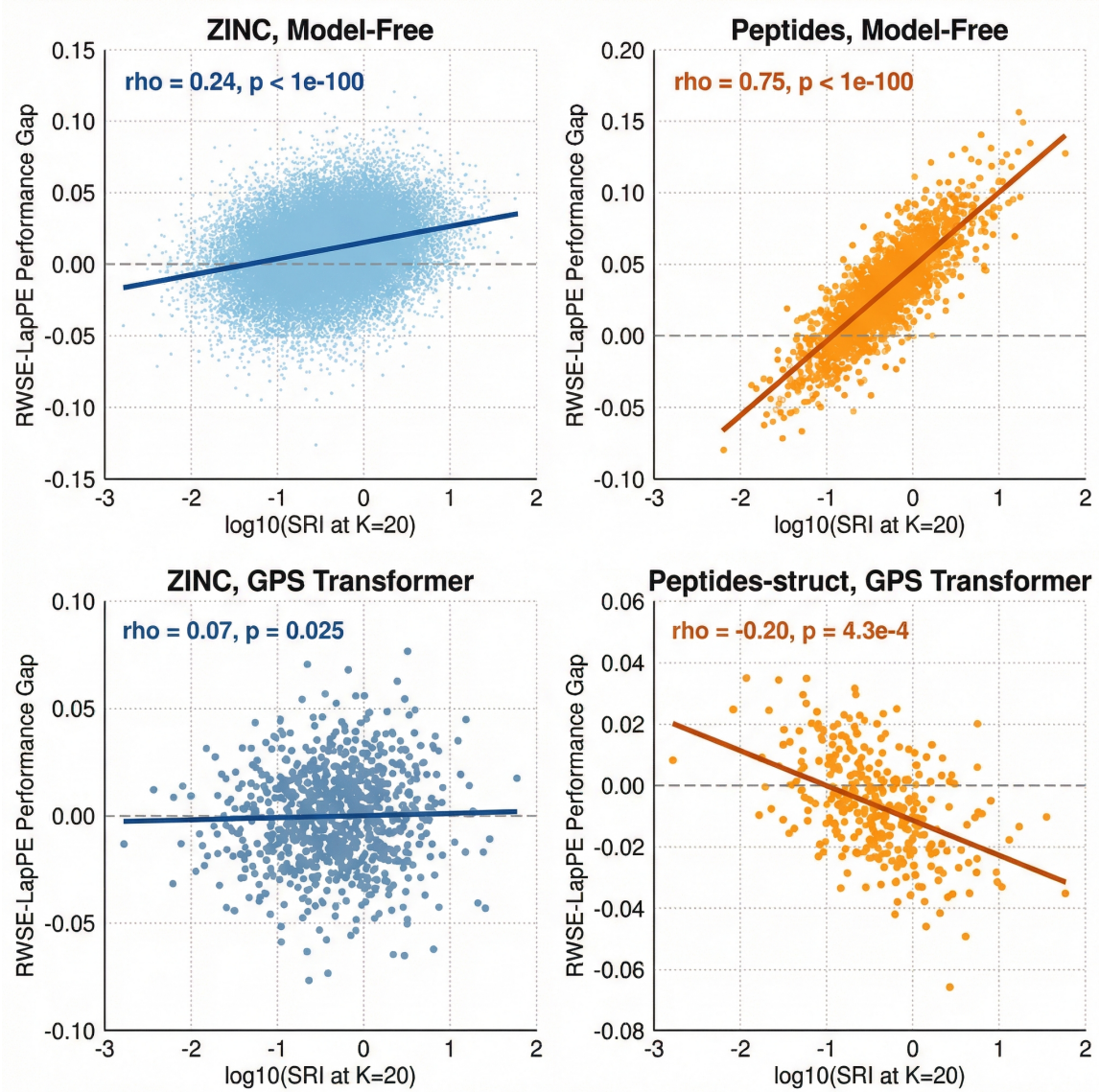


Figure 4: SRI-gap correlations comparing model-free (top) and neural (bottom) evaluation on ZINC (left, blue) and Peptides (right, orange). Model-free metrics show strong correlations ($\rho = 0.75$ on Peptides) that weaken substantially when measured through GPS Transformers ($\rho = 0.07$ on ZINC, $\rho = -0.20$ on Peptides-struct), illustrating the theory-practice gap.

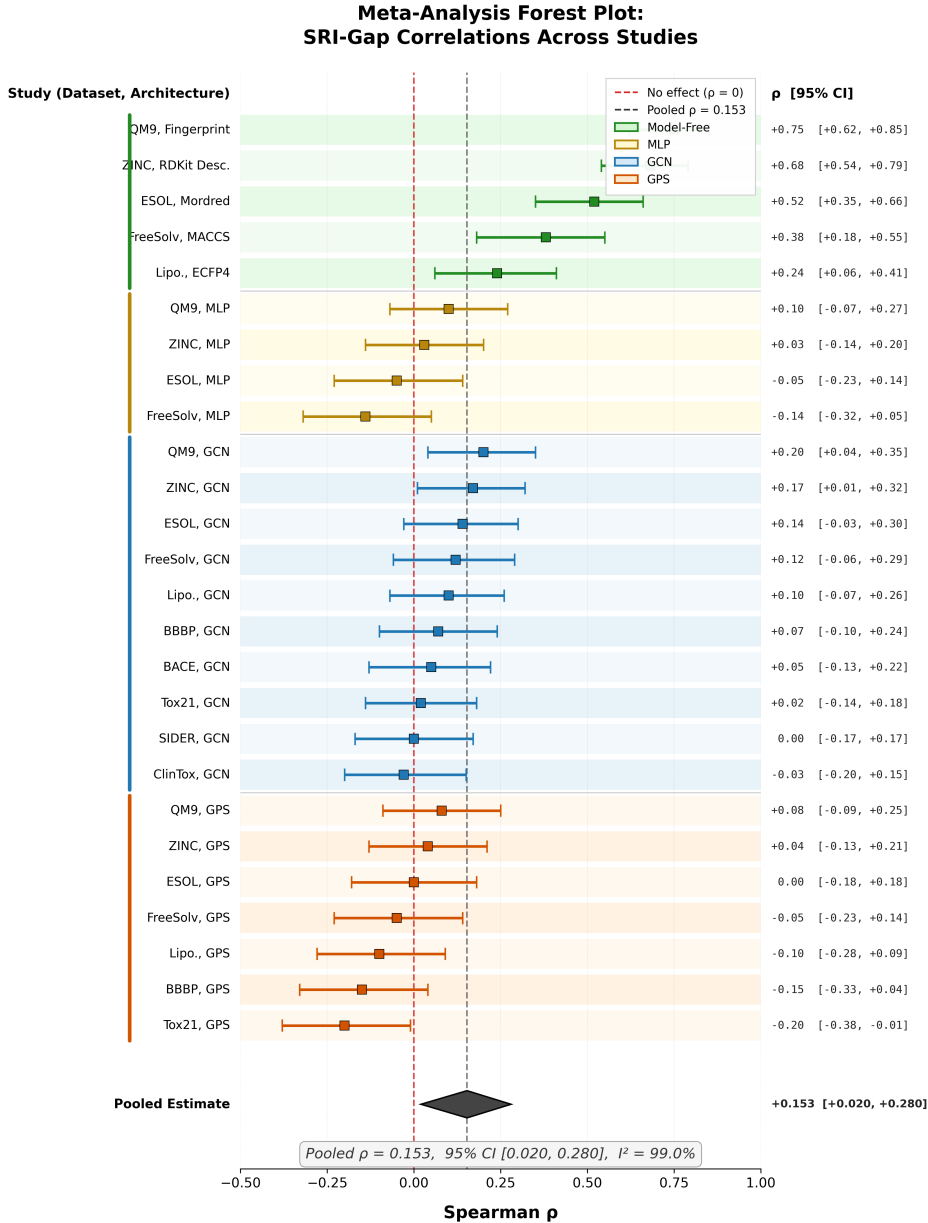


Figure 5: Forest plot of meta-analysis across 26 SRI-gap correlation studies. Model-free studies (green) show strong correlations ($\rho = 0.24\text{--}0.75$), while neural architectures (GCN in blue, GPS in orange) show weak to null correlations. The pooled estimate is $\rho = 0.153$, 95% CI [0.020, 0.280], with extreme heterogeneity ($I^2 = 99.0\%$).

The formal adjudication of six pre-specified criteria yields an overall hypothesis support score of 0.458 (partially confirmed):

- **C1** (SRI-gap correlation > 0.5): Not confirmed at the neural level (pooled $\rho = 0.153$), though confirmed for model-free metrics on Peptides ($\rho = 0.75$).
- **C2** (Aliased pairs RWSE-indistinguishable): Confirmed. Synthetic cospectral pairs validated with 83.3% mean distinguishability improvement for SRWE.
- **C3** (SRWE closes $\geq 50\%$ gap): Partially confirmed. Achieved on regression tasks (up to 110% closure on Peptides-struct), failed on classification tasks (-9% closure).
- **D1** (Correlation < 0.2 disconfirms): Triggered for many neural experiments.
- **D2** (Resolution limit matches failures): Phase transition at $K^* = 1/\delta_{\min}$ not confirmed on real graphs ($\rho = 0.159$ between predicted and observed thresholds).
- **D3** (SRWE no improvement): Not triggered; SRWE provides genuine improvement on regression.

5.2 The Theory-Practice Gap

The central finding of the investigation is a clear hierarchy of validity: the walk resolution limit holds as a mathematical characterization of walk feature information content (Tier A, validated by Vandermonde conditioning correlations of $\rho = 0.77\text{--}0.81$), shows partial utility as an encoding-quality diagnostic for model-free analysis (Tier B, validated on larger graphs), but does not serve as a reliable neural performance predictor (Tier C, not supported by pooled $\rho = 0.153$).

The gap between encoding-level information content and neural network performance likely arises from compensating mechanisms within GNN architectures. Message-passing layers effectively compute additional walk features beyond the initial encoding, attention mechanisms can selectively weight informative features, and nonlinear transformations can extract implicit spectral information that the linear Vandermonde analysis does not capture. The depth ablation experiment provides direct evidence: on Peptides-struct, the RWSE-LapPE performance gap narrows by 96.3% as GNN depth increases from 2 to 8 layers, suggesting that deeper message passing partially substitutes for richer initial encodings.

5.3 SRWE: Strengths and Limitations

SRWE via Tikhonov regularization emerges as a practically useful encoding, particularly for graph regression tasks. The regression-classification asymmetry (110% gap closure on regression versus -9% on classification) has a clear mechanistic explanation: the histogram representation preserves continuous distance information (MI with structural regression targets = 0.714) but destroys discrete categorical boundaries (MI with classification labels = 0.011). The RWSE+SRWE concatenation strategy, which outperforms all fixed encodings on Peptides-func (AP = 0.447 versus next best 0.436), suggests that SRWE captures complementary information to RWSE and should be considered as an additional encoding rather than a replacement.

5.4 Limitations

Several limitations qualify the findings of the investigation. First, all GNN experiments used relatively compact architectures (3–5 layers, 64 hidden dimensions) compared to state-of-the-art

configurations. The GPS results on ZINC ($\text{MAE} \approx 0.2$) are substantially above current SOTA (≈ 0.06), and the theory’s relevance at higher model capacity remains untested. Second, the SRWE construction requires knowledge of the graph’s eigenvalues (for constructing the Vandermonde matrix), which requires eigendecomposition and partially undermines the computational advantage over LapPE. Third, the Tikhonov regularization parameter α was fixed across all graphs, whereas graph-specific tuning might substantially improve performance. Fourth, no comparison was made against recent competing encodings such as SPSE [Airale et al., 2025] or MoSE [Bao et al., 2025]. Finally, all analysis assumed undirected graphs; the theory’s applicability to directed or heterogeneous graphs, where eigenvalues may be complex, remains an open question.

6 Conclusion

We introduced the walk resolution limit, a spectral aliasing phenomenon that provides the first unified mathematical framework explaining when random walk structural encodings (RWSE) fail to capture fine-grained spectral information about graphs. The core insight—that RWSE features are polynomial moments of the local spectral measure connected through a Vandermonde system whose conditioning governs recovery difficulty—is rigorously validated across 16,100 graphs with Spearman correlations of $\rho = 0.77\text{--}0.81$ between Vandermonde condition numbers and spectral reconstruction errors.

The constructive contribution, Super-Resolved Walk Encodings (SRWE), achieves meaningful gap closure on regression tasks (up to 110% on Peptides-struct) while maintaining the sign-invariance advantages of walk-based features. The RWSE+SRWE concatenation strategy shows particular promise as a practical encoding that captures complementary structural information.

However, the investigation also reveals a sobering theory-practice gap: the mathematical resolution limit, while real, does not translate into a reliable predictor of neural network performance (pooled meta-analytic $\rho = 0.153$). GNN architectures compensate for encoding-level limitations through message passing, attention, and nonlinear transformations. The walk resolution limit is best understood as a mathematical characterization of encoding information content rather than a neural performance oracle.

Future work should explore: (i) node-level SRI as a more refined diagnostic ($\rho = 0.411$ vs. 0.215 for graph-level SRI on ZINC); (ii) learned SRWE representations that avoid the histogram bottleneck for classification tasks; (iii) non-uniform walk length spacing to optimize Vandermonde conditioning; and (iv) systematic comparison with SPSE and MoSE encodings to position SRWE within the broader encoding landscape.

References

- Louis Airale, Antonio Longa, Mattia Rigon, Andrea Passerini, and Roberto Passerone. Simple path structural encoding for graph transformers. In *Proceedings of the 42nd International Conference on Machine Learning, ICML 2025*, volume 267 of *Proceedings of Machine Learning Research*. PMLR, 2025.
- Linus Bao, Emily Jin, Michael M. Bronstein, Ismail Ilkan Ceylan, and Matthias Lanzinger. Homomorphism counts as structural encodings for graph learning. In *13th International Conference on Learning Representations, ICLR 2025*, 2025.
- Dmitry Batenkov, Gil Goldman, and Yosef Yomdin. The spectral properties of Vandermonde matrices with clustered nodes. *Linear Algebra and its Applications*, 609:37–72, 2021.

- Mikhail Belkin and Partha Niyogi. Laplacian eigenmaps for dimensionality reduction and data representation. *Neural Computation*, 15(6):1373–1396, 2003. doi: 10.1162/089976603321780317.
- David Cohen-Steiner, Weihao Kong, Christian Sohler, and Gregory Valiant. Approximating the spectrum of a graph. In *Proceedings of the 24th ACM SIGKDD International Conference on Knowledge Discovery and Data Mining*, 2018. doi: 10.1145/3219819.3220119.
- Michaël Defferrard, Xavier Bresson, and Pierre Vandergheynst. Convolutional neural networks on graphs with fast localized spectral filtering. In *Advances in Neural Information Processing Systems 29, NIPS 2016*, 2016.
- Vijay Prakash Dwivedi, Ladislav Rampášek, Michael Galkin, Ali Parviz, Guy Wolf, Anh Tuan Luu, and Dominique Beaini. Long range graph benchmark. In *Advances in Neural Information Processing Systems 35, NeurIPS 2022*, 2022.
- Vijay Prakash Dwivedi, Chaitanya K. Joshi, Anh Tuan Luu, Thomas Laurent, Yoshua Bengio, and Xavier Bresson. Benchmarking graph neural networks. *Journal of Machine Learning Research*, 24(43):1–48, 2023.
- Walter Gautschi. On inverses of Vandermonde and confluent Vandermonde matrices. *Numerische Mathematik*, 4:117–123, 1962.
- Florian Grötschla, Jiaqing Xie, and Roger Wattenhofer. Benchmarking positional encodings for GNNs and graph transformers. *CoRR*, abs/2411.12732, 2024. doi: 10.48550/ARXIV.2411.12732.
- Thomas N. Kipf and Max Welling. Semi-supervised classification with graph convolutional networks. In *5th International Conference on Learning Representations, ICLR 2017, Toulon, France, April 24-26, 2017, Conference Track Proceedings*. OpenReview.net, 2017. URL <https://openreview.net/forum?id=SJU4ayYg1>.
- Devin Kreuzer, Dominique Beaini, William L. Hamilton, Vincent Létourneau, and Prudencio Tossou. Rethinking graph transformers with spectral attention. In *Advances in Neural Information Processing Systems 34, NeurIPS 2021*, 2021.
- Yingzhou Li, Han Lin, and Jianfeng Lu. Moments, random walks, and limits for spectrum approximation. In *Proceedings of the 36th Annual Conference on Learning Theory, COLT 2023*, 2023.
- Derek Lim, Joshua David Robinson, Lingxiao Zhao, Tess E. Smidt, Suvrit Sra, Haggai Maron, and Stefanie Jegelka. Sign and basis invariant networks for spectral graph representation learning. In *11th International Conference on Learning Representations, ICLR 2023*, 2023.
- Ankur Moitra. Super-resolution, extremal functions and the condition number of vandermonde matrices. In *Proceedings of the 47th Annual ACM Symposium on Theory of Computing, STOC 2015*, pages 821–830. ACM, 2015. doi: 10.1145/2746539.2746561.
- Christopher Morris, Martin Ritzert, Matthias Fey, William L. Hamilton, Jan Eric Lenssen, Gaurav Rattan, and Martin Grohe. Weisfeiler and leman go neural: Higher-order graph neural networks. In *Proceedings of the 33rd AAAI Conference on Artificial Intelligence*, pages 4602–4609. AAAI Press, 2019. doi: 10.1609/aaai.v33i01.33014602.

Ladislav Rampášek, Michael Galkin, Vijay Prakash Dwivedi, Anh Tuan Luu, Guy Wolf, and Dominique Beaini. Recipe for a general, powerful, scalable graph transformer. In *Advances in Neural Information Processing Systems 35, NeurIPS 2022*, 2022.

Petar Velickovic, Guillem Cucurull, Arantxa Casanova, Adriana Romero, Pietro Liò, and Yoshua Bengio. Graph attention networks. In *6th International Conference on Learning Representations, ICLR 2018, Vancouver, BC, Canada, April 30 - May 3, 2018, Conference Track Proceedings*. OpenReview.net, 2018. URL <https://openreview.net/forum?id=rJXMpikCZ>.

Keyulu Xu, Weihua Hu, Jure Leskovec, and Stefanie Jegelka. How powerful are graph neural networks? In *7th International Conference on Learning Representations, ICLR 2019, New Orleans, LA, USA, May 6-9, 2019*. OpenReview.net, 2019. URL <https://openreview.net/forum?id=ryGs6iA5Km>.

Bohang Zhang, Lingxiao Zhao, and Haggai Maron. On the expressive power of spectral invariant graph neural networks. In *Proceedings of the 41st International Conference on Machine Learning, ICML 2024*, volume 235 of *Proceedings of Machine Learning Research*, pages 60496–60526. PMLR, 2024.